Full Paper
doi.org/10.1002/ejic.202000437

Chemistry Europe
European Chemical Societies Publishing

Carbon Dioxide Activation

CO_2 Capture by 2-(Methylamino)pyridine Ligated Aluminum Alkyl Complexes

Timothy W. Yokley,[a][‡] Hrishikesh Tupkar,[a] Nathan D. Schley,[b] Nathan J. DeYonker,[a] and Timothy P. Brewster*[a]

Wiley Online Library

Abstract: A set of novel, easily synthesized aluminum complexes, Al[κ²-*N*,*N*-2-(methylamino)pyridine]$_2$R (R = Et, *i*Bu) are reported. When subjected to 1 atm of CO_2 pressure, each hemilabile pyridine arm dissociates and facilitates cooperative activation of the CO_2 substrate reminiscent of a Frustrated Lewis Pair. This reaction has limited precedent for Al/N based Lewis Pair systems, and this is the first system readily shown to sequester multiple equivalents of CO_2 per aluminum center. The ethyl variant then reacts further, inserting a third equivalent of CO_2 into the aluminum alkyl to generate an aluminum carboxylate. Examples of this type of reactivity are rare under thermal conditions. A joint experimental/computational study supports the proposed reaction mechanism.

Introduction

The concentration of atmospheric carbon dioxide has increased remarkably since the onset of the industrial revolution. A continued increase in the atmospheric concentration of this greenhouse gas will have long lasting effects on climate and the natural environment.[1] Efforts to quell the rising tide of CO_2 emission has led to extensive research into alternative energy sources,[2] carbon capture technology,[3] and biomass utilization.[4] The increased abundance and low cost of CO_2 also make it particularly attractive as a C_1 feedstock.[5] It presents a readily available, environmentally friendly alternative to the use of CO,[6,7] which is commonly produced in the energy intensive processes of coal gasification[8] or methane steam reforming.[9] However, the implementation of CO_2 as a chemical feedstock is challenging due to its high thermodynamic stability and its being relatively kinetically inert.[5,10,11] Processes that involve CO_2 typically require highly reactive substrates or severe reaction conditions, limiting the scope of desired transformations.

In nature, the Mg-containing Rubisco enzyme catalyzes CO_2 fixation during the Calvin Cycle.[12] Inspired by biological precedent, intense focus has been given to the development of organometallic catalysts that can insert CO_2 into metal-ligand bonds to generate chemically useful materials such as carbonates,[13,14] carbamates,[15,16] and carboxylic acids.[17] CO_2 has been observed to insert into a metal–alkyl bond of several *d*block and *p*-block alkyl complexes (M = Al, Mn, Fe, Co, Zn, Ru, In).[18–24] Of particular interest to our laboratory is the reactivity of aluminum complexes with CO_2, as the high Lewis acidity and oxophilic nature of the aluminum center make it likely to interact favorably with the substrate. Aluminum is also cheap and naturally abundant making it a prime candidate for large-scale implementation. Though not widely explored, the ability of CO_2 to insert into simple aluminum alkyls has been known since the 1960s.[25,26] These early examples were neither particularly efficient nor selective, but nonetheless demonstrated the potential of aluminum-based complexes for CO_2 fixation. Later advances with aluminum porphyrin systems increased reaction specificity but all required external base and visible light activation.[18,24] Building on this early work, Aldridge et al. have recently reported the synthesis of various -diketiminate stabilized aluminum hydrides [(Nacnac)Al(R)H; R = Me, Et, Cl, OTf], that demonstrate facile thermal CO_2 insertion into the Al–H bond when R is an electron donating group.[27]

In addition to the select complexes noted above, Frustrated Lewis Pairs (FLPs) have been observed to react productively with CO_2. Though boron-containing FLP systems are the most widely studied,[28–39] Menard and Stephan discovered that aluminum trihalides in the presence of sterically bulky phosphines could also facilitate CO_2 reduction, providing an alternate pathway to form CO or methanol.[40,41] Since then, several other aluminum-containing FLPs have been synthesized and tested for similar reactivity.[42–59] Notably, only two aluminumnitrogen Lewis pairs have been reported to bind CO_2;[43,60] the vast majority employ phosphorus as the Lewis basic element.[45–47,49,51–56] Mechanistically similar, cooperative CO_2 activation has also been observed in late transition metal-aluminum systems developed by Bourissou,[61] and Iwasawa and Takaya.[62] Notably, the recent report from Iwasawa and Takaya described a Pd-Al Z-type complex which catalyzed the hydrosil-

[a] *Dr. T. W. Yokley, H. Tupkar, Prof. Dr. N. J. DeYonker, Prof. Dr. T. P. Brewster*
Department of Chemistry, The University of Memphis
3744 Walker Ave., Memphis, TN 38152, USA
E-mail: tbrwster@memphis.edu
[b] *Prof. Dr. N. D. Schley*
Department of Chemistry, Vanderbilt University
Nashville, TN 37235, USA
[‡] Current address: Department of Chemistry, The Ohio State University
Columbus, OH 43210, USA

Supporting information and ORCID(s) from the author(s) for this article are available on the WWW under https://doi.org/10.1002/ejic.202000437.

2020

Full Paper
doi.org/10.1002/ejic.202000437

ylation of CO_2 with a turnover frequency (TOF) of 19300 h^{-1} under 1 atm of pressure, making it among the most efficient known catalysts for this transformation.[62] It is, however, noteworthy that while catalytic reduction of CO_2 has been achieved by a select few FLP systems, CO_2 sequestration by FLPs is largely limited to a single CO_2 molecule per Lewis acid.[47,54,56,62]

In this report, we demonstrate the ability of two novel aluminum alkyl complexes (Figure 1) to activate and capture multiple equivalents of CO_2 (relative to aluminum), an exciting and unusual reaction. The complexes are easily synthesized, accessible in good yield in a single step from commercial starting materials. CO_2 capture is found to proceed efficiently at room temperature without the need for chemical additives or any additional activation. Experimental and computational evidence suggest that CO_2 activation occurs in two ways; first, via a cooperative pathway in which a nitrogen atom from an associated pyridine works in concert with the aluminum center to trap the CO_2 molecule, and second, via a direct insertion into the alkyl ligand to form a carboxylate. This mechanism is consistent with those proposed in literature for related systems.[47,54,55]

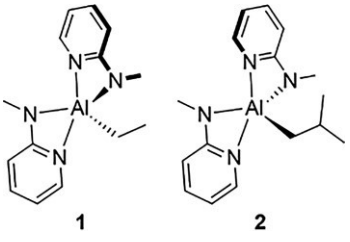

Figure 1. Newly synthesized aluminum complexes. Stereoisomers drawn to match crystal structure.

Synthesis and Characterization

Treatment of 2-(methylamino)pyridine (2.05 equivalents) with one equivalent of triethylaluminum or triisobutylaluminum at room temperature yielded di-aminopyridine-ligated aluminum alkyl complexes **1** and **2** (Figure 1) in moderate to good yield. Recrystallization from a concentrated solution of each in pentane at –35 °C led to recovery of moisture-sensitive white solids in high purity. Each complex has been characterized by standard spectroscopic and analytical techniques (See Experimental Details), and the molecular structures determined by X-ray crystallography (Figure 2, CCDC, accession numbers 1987618, 1987619). Both **1** and **2** are found to be monomeric in the solid state. The molecular geometry about aluminum is that of a distorted trigonal bipyramid with the pyridine-based nitrogen atoms occupying the pseudo-axial positions. The sum of equatorial bond angles in **1** and **2** are 359.82° and 360°, respectively. Solution characterization is consistent with the observed monomeric structure.

Attempts to synthesize and isolate monoligated aminopyridine-aluminum complexes were also made. However, when the synthesis is repeated with a 1:1 ratio of aminopyridine to aluminum, analytically pure di-ligated products **1** and **2** are obtained following recrystallization, even at low temperatures. This implies that the second addition of aminopyridine is rapid and

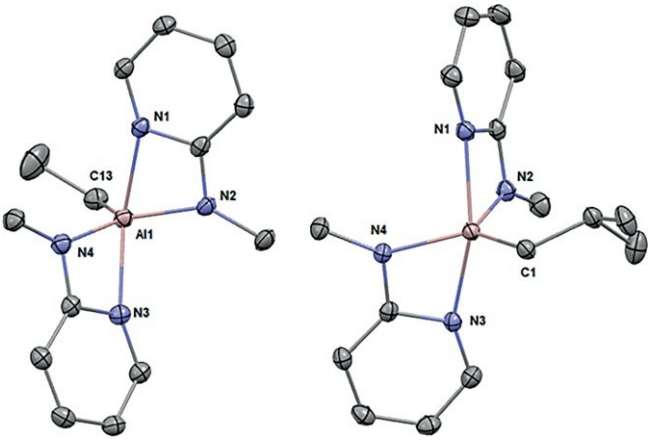

Figure 2. ORTEP representation of **1** (left) and **2** (right). Ellipsoids shown at 50 % probability. Hydrogen atoms omitted for clarity. Select bond lengths [Å] and angles [deg]: (**1**) N(1)pyridine–Al(1) 2.06(9), N(3)pyridine–Al(1) 2.11(0), N(2)–Al(1)–N(4) 119.33, C(13)–Al(1)–N(4) 117.26, C(13)–Al(1)–N(2) 123.23. (**2**) N(1)pyridine–Al(1) 2.085, N(3)pyridine–Al(1) 2.088, N(2)–Al(1)–N(4) 119.03, C(1)–Al(1)–N(2) 119.88, C(1)–Al(1)–N(4) 121.09. CCDC accession numbers 1987618, 1987619.

thermodynamically favorable or that ligand scrambling at low temperature leads to selective precipitation of the observed product.

Reactivity of Monometallic Aluminum Complexes with CO_2

The reactivity of **1** and **2** with 1 atm of CO_2 was then investigated at room temperature. Each complex was found to insert CO_2, though the exact nature of the final product was dependent on the alkyl group present in the complex. To achieve reaction, dry CO_2 was bubbled through a solution of the aluminum complex dissolved in 600 μL of [D_6]benzene in a screw-cap NMR tube for 5 minutes. The resulting mixture was then left to stand at room temperature CO_2 incorporation into the aluminum complex occurred readily. Spectroscopic evidence, generated first from ^{1}H NMR spectroscopy, suggests that the major product present after 24 hours is a symmetric cyclic carbamate, formed from insertion of CO_2 into both of the Al-$N_{pyridine}$ bonds (compounds **3** and **4**, Scheme 1). We assign this as the major

Full Paper
doi.org/10.1002/ejic.202000437

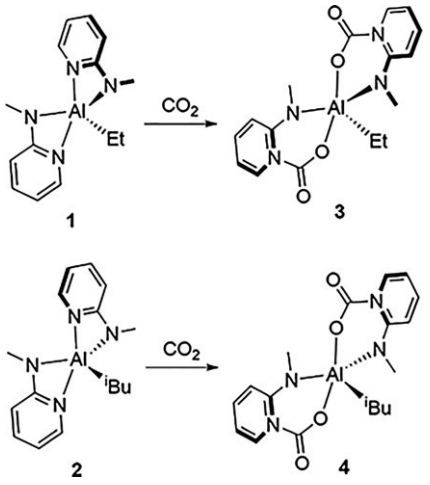

Scheme 1. Insertion of CO_2 into complexes **1** and **2**.

when the reaction is undertaken with isotopically labelled $^{13}CO_2$ suggesting that the resonance must derive from CO_2 insertion. ^1H-^{13}C HMQC and HMBC data further support our structural assignment; no proton-carbon coupling between the carbon signal at δ = 154 ppm and the alkyl proton resonances is apparent in either spectrum (See Supporting Information). Collectively, these data support our assignment of the reaction product as **3**. Similar analysis led to the assignment of the product of CO_2 addition to **2** as complex **4** (Figure 4).

Unfortunately, attempts to isolate the carbamate products and characterize them in the solid state were unsuccessful. There are two reasons for this. First, the aluminum alkyls are highly susceptible to hydrolysis from trace water which can enter the system through the screw-cap septum. Second, and more importantly, the insertion of CO_2 was observed to be reversible. Bubbling dry argon through an in situ generated crop of **3** and **4** led

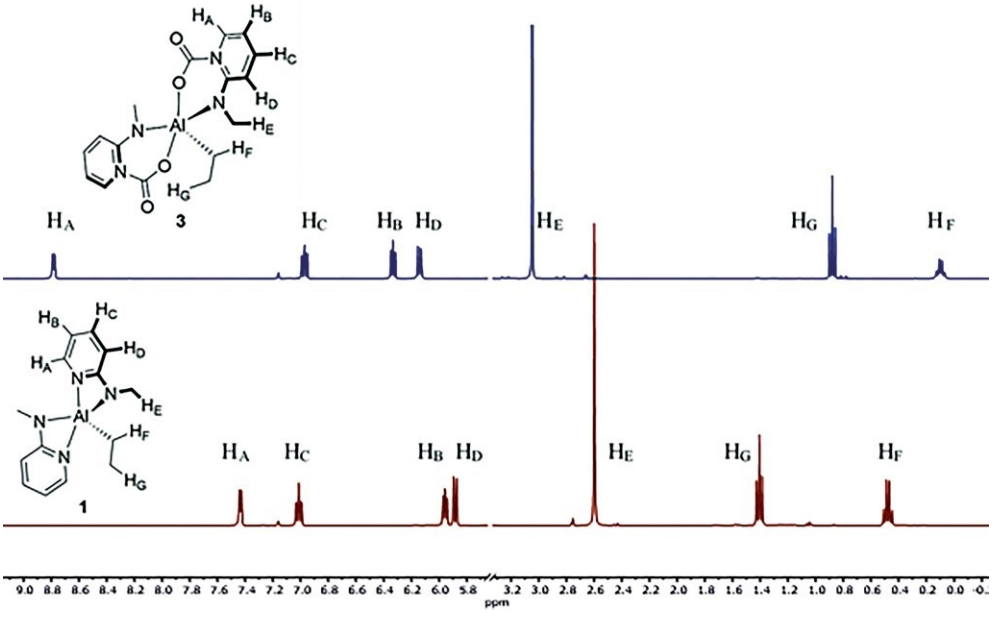

Figure 3. Stacked ^1H-NMR spectrum representative of **1** (bottom) and **3** after addition of 1 atm CO_2 (top) in [D_6]benzene. Spectra referenced to residual solvent peak (7.16 ppm).

product on the basis of three primary pieces of evidence. First, the NMR spectrum of the product (Figure 3, top) displays only one set of resonances attributable to the 2-(methylamino)pyridine ligand indicating that the complex must be symmetric or fluxional on the NMR time scale. Second, the resonance attributed to pyridine proton H_A (Figure 3) is observed to shift dramatically downfield from δ = 7.5 ppm to δ = 8.8 ppm. This suggests that the pyridine moiety is the most likely site of the observed reaction. Third, the methylene signal attributed to the ethyl group remains in the upfield region (δ = 0.10 ppm) associated with carbon ligands directly bound to electropositive atoms.

Further evidence for the identity of the product was obtained from $^{13}C\{^1H\}$ NMR spectroscopy. A new downfield peak, observed at δ = 154 ppm in the spectrum, is indicative of the carbonyl carbon in the corresponding carbamate product. This peak is enhanced

to the reversion of the complexes back to **1** and **2** (along with a small amount of hydrolysis). The observation of reversible CO_2 insertion is consistent with our computational analysis (see below) in which insertion is slightly endergonic in the absence of second-sphere CO_2. Crystal growth in the glovebox under an atmosphere of CO_2 did not yield suitable single crystals for X-ray analysis.

In an effort to better understand the observed reactivity, we monitored the progress of the reaction of **1** with isotopically labelled $^{13}CO_2$ over extended times. Reactions were run in screw-cap NMR tubes by the method described above and monitored by $^{13}C\{^1H\}$ NMR spectroscopy. Full conversion to the doubly inserted carbamate was observed in 90 minutes. Signals corresponding to a singly inserted carbamate were not observed, suggesting that the second CO_2 capture event proceeds rapidly after the first. To our surprise, after exposing **1** to CO_2 for 48 hours, a new isotopically enhanced peak was observed to appear at δ = 173 ppm in the $^{13}C\{^1H\}$ NMR spectrum. We suspect that this new peak arises from further CO_2 insertion into the aluminum ethyl to form an aluminum-

Full Paper
doi.org/10.1002/ejic.202000437

bound propionate. After 72 hours, the new carbonyl peak remains prominent in the $^{13}C\{^1H\}$ NMR spectrum suggesting the compound is stable at room temperature and does not decarbonylate to produce alkoxide as has been observed in other systems.[41] Unfortunately, attempts to crystallize this final product were unsuccessful.

Subjecting the isobutyl derivative **2** to similar reaction conditions does not yield the corresponding pentanoate. While the bis-carbamate similarly forms readily, it remains stable in solution for several days (96 hours monitored by ^1H & $^{13}C\{^1H\}$-NMR spectroscopy) before degrading into an undesirable side product. Upon analysis of the product spectra, we postulated that the eventual decomposition product is the hydrolyzed form of the aluminum carbamate species. To verify this hypothesis, we intentionally reacted the generated carbamate with 5 μL of water and compared the resultant ^1H NMR spectrum with that of the final decomposition product. A distinct doublet located at δ = 8.21 ppm serves as a diagnostic resonance for the hydrolysis product (See Figure S17 in Supporting Information). This directly matches a resonance observed in our CO_2 insertion experiments 5 hours after the addition of CO_2 (≈ 13 % by ^1H-NMR integration). Additionally, a doublet located at δ = 0.86 ppm in the ^1H NMR spectrum, corresponding to the methyl protons of isobutane, is observed to increase in magnitude over the course of our CO_2 insertion experiments indicating hydrolysis of the alkyl is occurring over time. This undesired by-product is not surprising. Reaction of aluminum alkyls with adventitious water is well known to occur rapidly under most conditions; slow contamination of our reaction mixture through the punctured NMR septum cap would be expected to result in its formation after long periods of time.

The combined results from the reactions described above led us to hypothesize a mechanistic theory as to how CO_2 insertion would occur. First, the hemilabile pyridine arm of the substituted pyridine ligand dissociates from the aluminum center. This is quite likely due to the geometrically strained 4-membered ring formed on κ^2 binding of 2-(methylamino)pyridine. CO_2 is then cooperatively activated by the Lewis pair to generate a cyclic carbamate. This cooperative reactivity is reminiscent of that described by Stephan,[40] Fontaine,[55] and Uhl[43] for AlP FLPs and by Gellrich[34] for a pyridonate-boron analogue. Subsequent insertion into the aluminum alkyl could then happen by one of two ways. First, CO_2 could directly insert into the alkyl ligand. Alternatively, CO_2 could migrate from the carbamate moiety to the aluminum alkyl before capture of a third equivalent of CO_2 by the now-accessible pyridine.

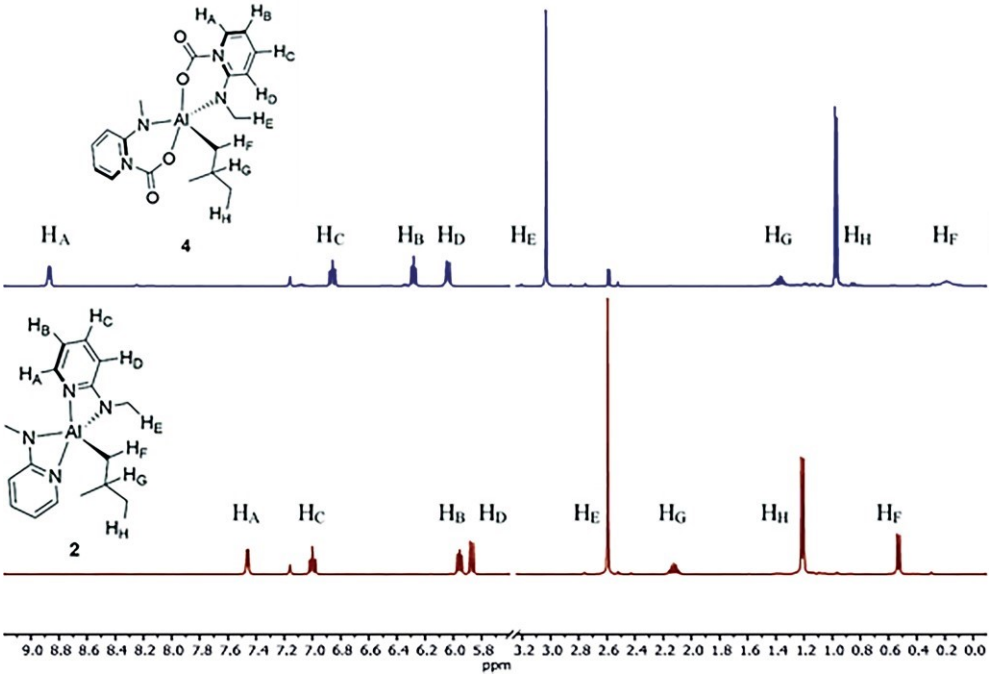

Figure 4. Stacked ^1H-NMR spectrum representative of **2** (bottom) and **4** after addition of 1 atm CO_2 (top) in [D_6]benzene. Spectra referenced to residual solvent peak.

Computational Investigation of the Mechanism

To further refine our mechanistic hypothesis, a computational study was undertaken. We sought to determine the overall reaction pathway for generation of **8**, the final triply inserted product derived from **1** (Figure 5), by answering two central questions. First, into which ligand is CO_2 insertion favored for the starting material and each potential reaction intermediate? And, second, can CO_2 migrate between ligands after insertion? Reasonable transition states could not be located for CO_2 migration at any point in the reaction sequence, thus, overall computed pathways (Figure 5) involved (1) insertion of CO_2 into the alkyl, followed by insertion into the pyridine to form a carbamate, (2) insertion into a single pyridine ligand followed by insertion into the alkyl, followed by insertion into the second pyridine, and (3) insertion into successive pyridine ligands followed by insertion into the alkyl. While observation of intermediate **3** suggests against

Full Paper
doi.org/10.1002/ejic.202000437

pathways 1 and 2, reversible de-insertion of CO_2 from the bis-carbamate would plausibly allow access to these routes.

Complicating our computational analysis is the ability of the aluminum complex to stereochemically isomerize. The pyridine nitrogen atoms can exist in the two axial positions of the trigonal bipyramid (**1-trans**, as seen in the crystal structure of **1**), 2 equatorial positions, or one axial and one equatorial (**1-cis**). In solution, the two methylaminopyridine ligands are found to be chemically equivalent on the NMR timescale, but this does not preclude rapid isomerization. In Figure 6, the optimized 3D structures of **1-trans** and **1-cis** are shown. Theoretically, **1-cis** is only 2.2 kcal/mol higher in free energy than **1-trans**. In Figure 7, a free energy diagram is provided, showing that the **1trans** form can isomerize to **1-cis** through a high-energy intermediate (**1-i**). The rate-limiting step has a barrier of 12.6 kcal/ mol, and the reverse activation free energy from **1-cis** to **1-i** is 9.0 kcal/mol. Accordingly, this interconversion should be rapid at the experimental conditions. However, for brevity, we have opted to avoid mapping out the complete reaction network of proposed *cis*/*trans* interconversion mechanisms. Unlike studies where examination of the full reaction network contributes

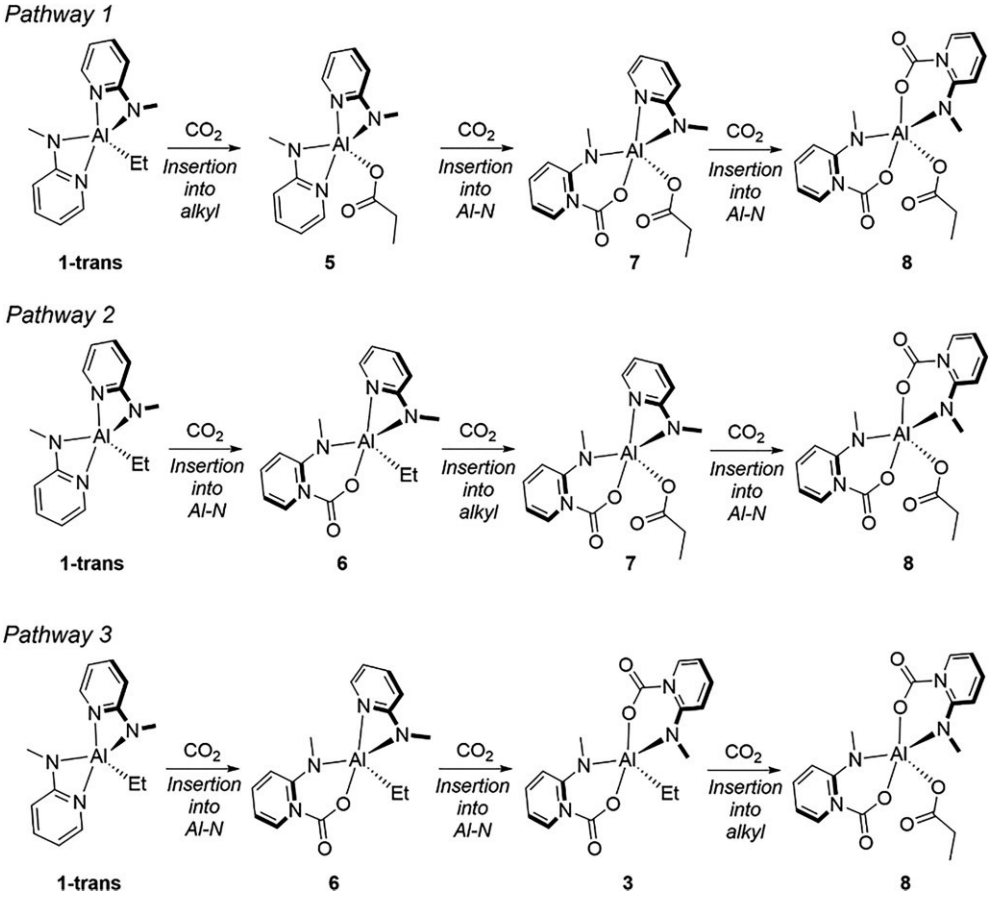

Figure 5. Computed reaction pathways for sequential CO_2 insertion into complex **1**.

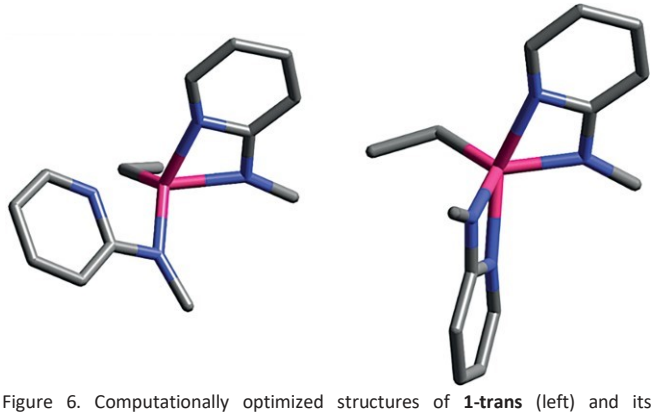

Figure 6. Computationally optimized structures of **1-trans** (left) and its counterpart **1-cis** (right), where the methyl substituents of the aminomethylpyridine are sterically unfavored. Hydrogen atoms are removed for clarity.

Full Paper
doi.org/10.1002/ejic.202000437

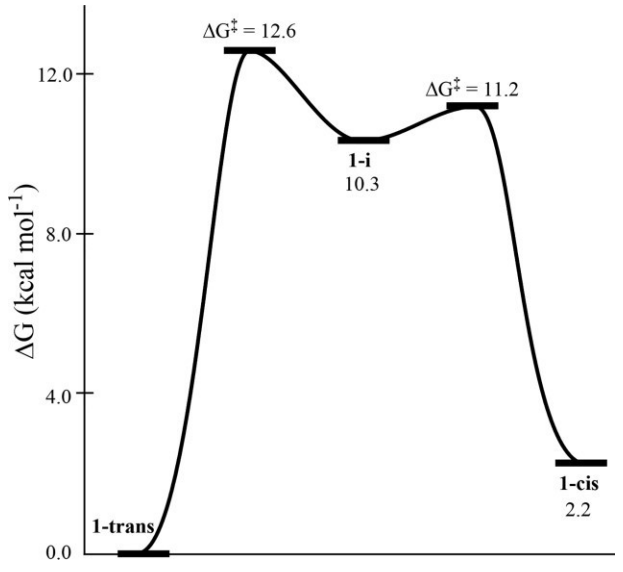

Figure 7. Free energy diagram of proposed isomerization of reactant **1** from *trans* to *cis* form. The reference free energy (in kcal/mol) is that of the **1-trans** structure.

greatly to an understanding of the observed kinetics and thermodynamics,[63,64] the ability of the various stereoisomeric forms of each complex to interconvert is simply assumed to be possible based on the low barrier to isomerization calculated for **1**. The lowest energy, spectroscopically consistent "*trans*" complexes accurately reflect the experimental data and are presented in detail below.

The free energy diagram of proposed Pathway 1 is provided in Figure 8. Formation of the various aluminum complex + CO_2 supermolecules are electronically favored by 15–20 kcal/mol compared to the infinitely separated components in all proposed mechanisms. Along the reaction coordinate of Pathway 1, the first elementary step entails CO_2 insertion into the alkyl group of complex **1**. The computed free energy of activation for this initial step is high, with $\Delta G^{\ddagger}$ = 34.4 kcal/mol. The unfavorable kinetics leading to intermediate **5** do not correspond to experimental observations of product formation on the timescale of minutes. Unlike the formation of intermediate **5**, subsequent insertion of a second CO_2 molecule into the Al–N bonds of the 2-methylamino ligand (to form intermediate **7a**) is endergonic, $\Delta\Delta G$ = +10.9 kcal/mol. Considering the conformational rearrangement from **7a** to **7**, the free energy to convert **5** + CO_2 to **7** is still uphill, with $\Delta\Delta G$ = +5.4 kcal/mol However, the irreversible and highly exergonic formation of **5**, coupled with the precedent that our chosen level of theory may overestimate activation energies for Al-containing systems by a few kcal/ mol,[65] suggests that formation of the intermediate **7a** may be facile.

Various intermediates connecting **5** and **7** are not likely minima on the room temperature free energy surface but are still discrete minima corresponding to conformational changes on the 0 K, vibration-less DFT energy surface. It is necessary to identify these structures on the free energy diagram to adhere to the Principle of Microscopic Reversibility.[66] 3D structures for intermediates **7a**, **7b**, **7c**, and **7** are displayed in Figure S21. Intermediate **7a** converts to **7b** via rotation of the propanoate ligand along to Al–O axis. Next, the carbamate ligand of **7b** puckers to form intermediate **7c**. Finally, the propanoate ligand binds in a κ^2 fashion to the aluminum center

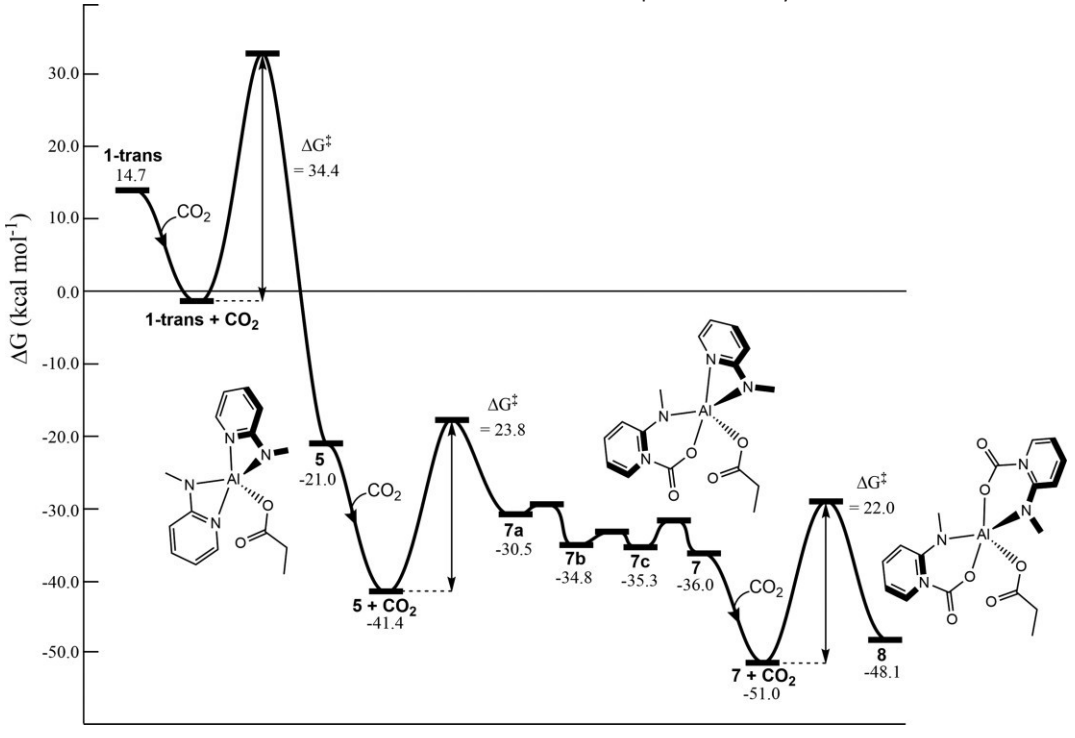

Figure 8. Free energy diagram of proposed activation of CO_2 to the aluminium-bound carboxylate where CO_2 insertion into alkyl group occurs first (Pathway 1 in Figure 5). The baseline free energy (in kcal/mol) is complex **1** + the free energy of CO_2 at infinite separation.

Full Paper
doi.org/10.1002/ejic.202000437

to form intermediate **7**. Addition of a third CO_2 molecule to form the product **8** is also endergonic compared to the **7** + CO_2 supermolecular complex by 2.9 kcal/mol, and the activation free energy is 22.0 kcal/mol. Based on the free energy diagram of Figure 8, it would be expected that complex **5** and various conformers of **7** could form minor products from reactant **1** over long timescales, and eventually funnel to product **8**. However, we will continue to show that Pathway 1 is not the most kinetically or thermodynamically viable pathway.

We then turned our attention to Pathway 2. No transition states leading between **6** and **7** were able to be characterized theoretically, and no transition states were located where CO_2 groups on the carbamate could migrate then insert into the Al–alkyl bond. These unsuccessful transition state searches rule out Pathway 2 and minimize the possibility of facile interconversion among the three pathways shown in Figure 5.

We last examined Pathway 3, whose free energy diagram is shown in Figure 9. Note that the supermolecular complex **1-trans** + CO_2 in Figure 9 has a slightly different conformation than the one in Figure 8, and thus has a slightly different relative free energy to the infinitely separated reactants. It is clear that CO_2 insertion into the Al–N bond described in pathway 3 has favorable kinetics as compared to the alkyl insertion in Pathway 1. The transition state for CO_2 insertion to form intermediate **6** has an activation free energy of only 16.4 kcal/mol. Interestingly, unlike the thermodynamics of Pathway 1, the elementary step of the first CO_2 insertion is endergonic by 4.8 kcal/mol. Insertion of the second CO_2 into the other Al–N bond of complex **6** to form complex **3** has an activation free energy of 20.4 kcal/mol. This reaction is the most endergonic step in either proposed Pathways 1 or 3, with a $\Delta\Delta G$ of +11.5 kcal/mol. However, stabilization by CO_2 in the computed supermolecule **3 + CO_2** suggests that **3** should form readily in the presence of excess CO_2. This is consistent with experimental observation of **3** in solution and the difficulty in isolating **3** in the solid state.

Finally, the third CO_2 insertion, into the Al–C bond, has an effective activation free energy of 30.5 kcal/mol, which is qualitatively lower than the first elementary step in Pathway 1 (34.4 kcal/mol). Similar to Pathway 1, the formation of a propionate ligand in Pathway 3 is extremely exothermic/exergonic ($\Delta\Delta G$ = –29.2 kcal/mol). The significant difference within the proposed Pathway 3 is that CO_2 insertion into the Al–alkyl bond is the final elementary step, resulting in favorable thermodynamics for formation of experimentally observed product **8**. Long reaction times required for the formation of **8** are also consistent with this step having a high effective barrier. Thus, Pathway 3 appears to be most likely mechanism.

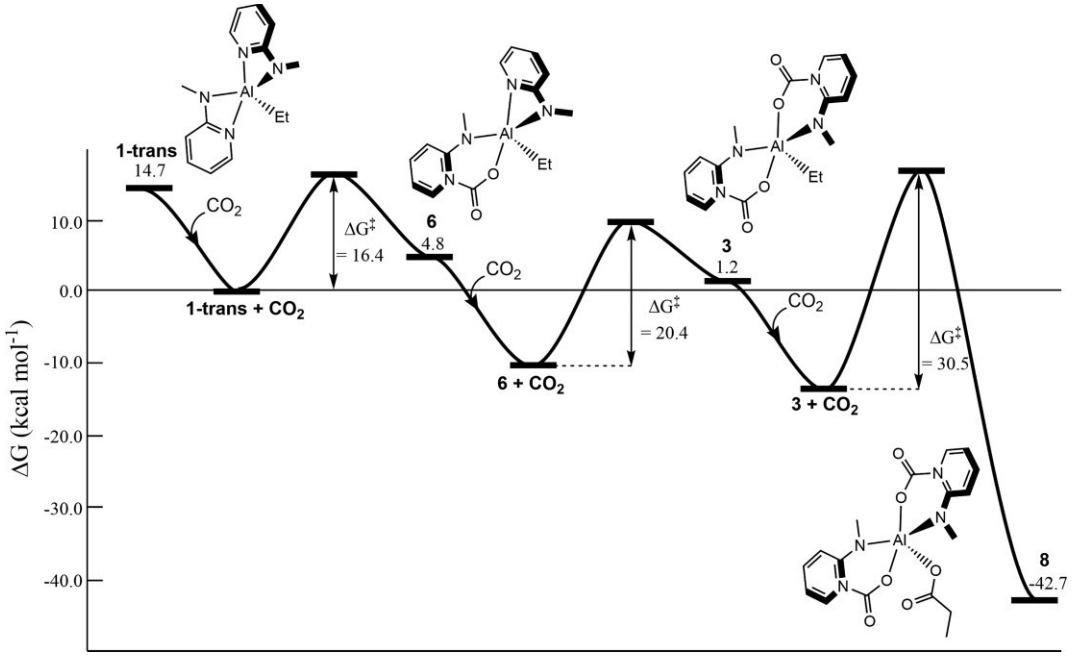

Figure 9. Free energy diagram of proposed activation of CO_2 to the aluminum bound carboxylate (Pathway 3). The baseline free energy (in kcal/mol) is **1-trans** + the free energy of CO_2 at infinite separation.

Conclusion

We have demonstrated the ability to cooperatively activate and capture CO_2 using simple organoaluminum complexes at room temperature. Addition of CO_2 to [2-(methylamino)pyridine]$_2$AlR (R = Et, *i*Bu) led to the clean formation of a bis-metalocyclic carbamate product. In the case of [2-(methylamino)pyridine]$_2$AlEt, we were able to observe additional insertion of CO_2 into the aluminum ethyl moiety at long reaction times. Three different proposed mechanisms were explored. Pathway 1, where the first CO_2 inserts into the aluminum–alkyl bond, could be competitive. However, computational evidence suggests that this pathway is not dominant and that formation of intermediates with only one or two CO_2

adducts slowly form thermodynamically favorable minor products. We conclude that the final product forms by way of direct CO_2 insertion into the aluminum alkyl, yielding an aluminum bound propionate, *only after* two carbamate ligands have been formed from the first two CO_2 insertions. Exploration of additional aluminum systems for CO_2 activation is ongoing in the laboratory.

Experimental Section

General Considerations

Syntheses and manipulations were performed in a nitrogen-filled Inert Technologies glovebox or using standard Schlenk techniques unless otherwise specified. Deuterated solvents were purchased from Cambridge Isotope Laboratories, dried with molecular sieves or calcium hydride, and stored in the glovebox over molecular sieves prior to use. CO_2 was passed through a Drierite column to remove trace water. $^{13}CO_2$ was purchased from Sigma-Aldrich. All other reagents and solvents used were commercially available and used without further purification unless specified. Aluminum reagents and 2-(methylamino)pyridine were stored in a nitrogen glovebox prior to use. NMR spectra were recorded on a 400 MHz JEOL spectrometer and referenced to the residual solvent peak.[67] (NOTE: All newly synthesized complexes are extremely reactive with atmospheric moisture which prevented reliable elemental analysis data from being acquired. Purity was assessed by ^{1}H NMR spectroscopy and mass confirmation was acquired using HRMS data acquired on a Waters Synapt High Resolution Mass Spectrometer. See Supporting Information for NMR spectra and HRMS raw data.)

Synthesis of Al(Et)(2-methylamino pyridine)$_2$ (1): In the glovebox, a solution of Al(Et)$_3$ (1 mL, 7.3 mmol) in 10 mL of THF was prepared. The solution was removed from the glovebox and 2methylamino pyridine 1.578 g (1.5 mL, 14.6 mmol) was added. Rapid bubbling was observed, indicating liberation of ethane gas. A pale-yellow solution resulted after ten minutes. The solution was then allowed to stir at room temperature for 24 hours. Solvent was removed in vacuo to yield a pale yellow solid. The solid was washed with pentane (3 × 3 mL) and dried in vacuo. A second crop of product crystals was grown by placing the pentane wash in the glovebox freezer (–35 °C) overnight. Yield: 1.3024 g, 66 %. ^{1}H NMR (400 MHz, [D$_6$]benzene) δ = 7.43 (dt, *J* = 5.1, 1.1 Hz, 2H), 7.01 (dd, *J* = 7.0, 1.6 Hz, 2H), 5.95 (m, 2H), 5.88 (d, *J* = 8.6 Hz, 2H), 2.60(s, 6H) 1.42 (t, *J* = 8.1 Hz, 3H) 0.48 (q, *J* = 8.4 Hz, 2H). ^{13}C{^{1}H} NMR (101 MHz, [D$_6$]benzene) δ = 167.47, 143.70, 140.30, 107.54, 102.67, 29.51, 10.25. [Aluminum alkyl CH_2 absent from ^{13}C{^{1}H} NMR spectrum due to quadrupolar relaxation.] HRMS calculated for $[C_{12}H_{16}AlN_4O]^+$; $[M + H]^+$; (product of alkyl hydrolysis) *m/z calcd.* 259.1140, found 259.1333.

Synthesis of Al(*i*Bu)(2-methylamino pyridine)$_2$ (2): In the glovebox, a solution of Al(*i*Bu)$_3$ (1 mL, 3.96 mmol) in 10 mL of THF was prepared. The solution was removed from the glovebox and 0.857 g of 2-methylamino pyridine (0.81 mL, 7.92 mmol) was added. Rapid bubbling was observed, indicating liberation of isobutane gas. A pale-yellow solution resulted after ten minutes. The solution was then allowed to stir at room temperature for 24 hours. Solvent was removed in vacuo to yield a pale yellow solid. The solid was washed with pentane (3 × 3 mL) and dried in vacuo. A second crop of product crystals was grown by placing the pentane wash in the glovebox freezer (–35 °C) overnight. Yield: 0.95 g, 80 %. ^{1}H NMR (400 MHz, [D$_6$]benzene) δ = 7.40 (d, *J* = 5.3 Hz, 2H), 6.95 (dd, *J* = 7.2, 1.7 Hz, 2H), 6.00–5.89 (m, 2H), 5.80 (d, *J* = 8.6 Hz, 2H), 2.59 (s, 6H), 2.05 (nonet, *J* = 6.6 Hz, 1H), 1.21 (d, *J* = 6.5 Hz, 6H), 0.53 (d, *J* = 6.9 Hz, 2H). ^{13}C{^{1}H} NMR (101 MHz, [D$_6$]benzene) δ = 167.36, 143.60, 140.28, 107.55, 102.70, 29.37, 28.02, 27.02. [Aluminum alkyl CH_2 absent from ^{13}C{^{1}H} NMR spectrum due to quadrupolar relaxation.] HRMS calculated for $[C_{16}H_{23}AlN_4]^+$; $[M]^+$; *m/z calcd.* 298.1738, found 298.1624.

***In situ* Generation of (2-Methylamino pyridine)$_2$Al(Et)(CO$_2$)$_2$ (3):** In the glovebox, approximately 12 mg of **1** was weighed inside a vial, dissolved in 600 μL of [D$_6$]benzene, and transferred inside a screw cap NMR tube. The tube was removed from the box and dry CO_2 was bubbled through the solution for 5 minutes. ^{1}H NMR (400 MHz, [D$_6$]benzene) δ = 8.78 (dd, *J* = 5.8, 1.6 Hz, 2H), 6.97 (m, 2H), 6.33 (m, 2H), 6.14 (d, *J* = 8.7 Hz, 2H), 3.05 (s, 6H). 0.88 (t, *J* = 8.1 Hz, 3H), 0.10 (q, *J* = 8.1 Hz, 2H). ^{13}C{^{1}H} NMR (101 MHz, [D$_6$]benzene) δ = 154.11, 152.71, 145.83, 140.62, 116.48, 111.93, 34.37, 9.85. [Aluminum alkyl CH_2 absent from ^{13}C{^{1}H} NMR spectrum due to quadrupolar relaxation.]

In situ Generation of (2-Methylamino pyridine)$_2$Al(*i*Bu)(CO$_2$)$_2$ (4): In the glovebox, approximately 12 mg of **2** was weighed inside a vial, dissolved in 600 μL of [D$_6$]benzene, and transferred inside a screw cap NMR tube. The tube was removed from the box and dry CO_2 was bubbled through the solution for 5 minutes. ^{1}H NMR (400 MHz, [D$_6$]benzene) δ = 8.87 (dd, *J* = 5.8, 1.6 Hz, 2H), 6.86 (ddd, *J* = 9.0, 7.3, 2.0 Hz, 2H), 6.28 (ddd, *J* = 6.9, 5.7, 1.0 Hz 2H), 6.14 (d, *J* = 8.7 Hz, 2H), 3.05 (s, 6H), 1.38 (m, 1H), 0.97 (d, *J* = 6.5 Hz, 6H), 0.10 (br, 2H).

X-ray Crystallography

A suitable crystal of each sample was selected for analysis and mounted in a polyimide loop. All measurements were made on a Rigaku Oxford Diffraction Supernova Eos CCD with filtered Cu-K_α radiation at a temperature of 100 K. Using Olex2,[68] the structure was solved with the ShelXT structure solution program using Direct Methods and refined with the ShelXL refinement package[69] using Least Squares minimization. All structures were refined without restraint. Structures have been uploaded to the CCDC, deposition numbers 1987618, 1987619.

Deposition Numbers 1987618, 1987619 contain the supplementary crystallographic data for this paper. These data are provided free of charge by the joint Cambridge Crystallographic Data Centre and Fachinformationszentrum Karlsruhe Access Structures service www.ccdc.cam.ac.uk/structures.

Computational Details

All computations were performed using the Gaussian16 software package.[70] Gas-phase energies, optimized geometries, and unscaled harmonic vibrational frequencies were obtained using Density Functional Theory (DFT).[71] The pure hybrid B3LYP functional was used with default grid parameters.[72] The basis set for aluminum was the standard Hay and Wadt basis set and effective core potential (ECP) combination (LANL2DZ)[73,74] All carbon, nitrogen, oxygen, and hydrogen atoms utilized the 6-31G(d′) basis set.[75] Spherical harmonic d functions were used throughout; i.e., there are five angular basis functions per d function. The Hessian of the energy was computed at all stationary points to confirm if they were minima (no imaginary vibrational frequencies) or transition states (only one imaginary vibrational frequency). Unscaled harmonic vibrational frequencies, zero-point energies (ZPE) and thermal enthalpy/free energy corrections were computed at 1 atm and 298.15 K. Solvation energies

were computed using the CPCM model with standard cavity parameters for benzene.[76,77]

Acknowledgments

This work was supported in part by the National Institutes of Health (NIH-NIGMS) under award number 1R21GM134339 (T.P.B., T.W.Y.) and in part by a grant from The University of Memphis College of Arts and Sciences Research Grant Fund (T.P.B). This support does not necessarily imply endorsement by the University of research conclusions. N. J. D. and H. T. were partially supported by start-up funding from the University of Memphis Department of Chemistry and N. J. D. was partially supported by the National Science Foundation under CAREER Grant BIO-1846408. Computational work was performed using resources at the University of Memphis High-Performance Computing Facility and the Computational Research on Materials Institute at the University of Memphis (CROMIUM). NMR data was obtained on an instrument acquired via NSF-MRI Grant No. CHE-1531466. Mr. Drake Williams is acknowledged for assistance in collecting High Resolution Mass Spectrometry data.

Keywords: Aluminum · Carbon dioxide · Frustrated Lewis pair · Insertion · Carbamate

[1] R. Kohut, *Environment Int.* **2003**, *29*, 171–180.
[2] J. Mohtasham, *Energy Procedia* **2015**, *74*, 1289–1297.
[3] Y. Liu, Z. U. Wang, H. C. Zhaou, *Greenh. Gases* **2012**, *2*, 239–259.
[4] S. Pang. *Fuel Flexible Gas Production: Biomass, Coal, and Bio-Solid Wastes in Fuel Flexible Energy Generation* (Ed.: J. Oakey) Woodhead Publishing **2016**, pp. 241–269.
[5] M. Aresta, A. Dibenedetto, *Dalton Trans.* **2007**, 2975–2992.
[6] Q. Liu, L. Wu, R. Jackstell, M. Beller, *Nat. Commun.* **2015**, *6*, 5933.
[7] A. Behr, *Angew. Chem. Int. Ed. Engl.* **1988**, *27*, 661–678; *Angew. Chem.* **1988**, *100*, 681–698.
[8] S. J. Self, B. V. Reddy, M. A. Rosen, *Int. J. Energy Environ. Eng.* **2012**, *13*, 16.
[9] J. P. Van Hook, *Catal. Rev.* **1980**, *21*, 1–51.
[10] H. Arakawa, M. Aresta, J. N. Armor, M. A. Barteau, E. J. Beckman, A. T. Bell, J. E. Bercaw, C. Creutz, E. Dinjus, D. A. Dixon, K. Domen, D. L. DuBois, J. Eckert, E. Fujita, D. H. Gibson, W. A. Goddard, D. W. Goodman, J. Keller, G. J. Kubas, H. H. Kung, J. E. Lyons, L. E. Manzer, T. J. Marks, K. Morokuma, K. M. Nicholas, R. Periana, L. Que, J. Rostrup-Nielson, W. M. H. Sachtler, L. D. Schmidt, A. Sen, G. A. Somorjai, P. C. Stair, B. R. Stults, W. Tumas, *Chem. Rev.* **2001**, *101*, 953–996.
[11] E. E. Benson, C. P. Kubiak, A. J. Sathrum, J. M. Smieja, *Chem. Soc. Rev.* **2009**, *38*, 89–99.
[12] I. Andersson, A. Backlund, *Plant Physiol. Biochem.* **2008**, *46*, 275–291.
[13] R. Zevenhoven, S. Eloneva, S. Teir, *Catal. Today* **2006**, *115*, 73–79.
[14] T. Sakakura, K. Kohno, *Chem. Commun.* **2009**, 1312–1330.
[15] Q. Zhang, H. Y. Yuan, N. Fukaya, H. Yasuda, J. C. Choi, *Green Chem.* **2017**, *19*, 5614–5624.
[16] A. Ion, C. Van Doorslaer, V. Parvulescu, P. Jacobs, D. De Vos, *Green Chem.* **2008**, *10*, 111–116.
[17] A. H. Liu, B. Yu, L. N. He, *Greenh. Gases* **2014**, 1–17.
[18] T. Aida, S. Inoue, *J. Am. Chem. Soc.* **1983**, *105*, 1304–1309.
[19] T. Arai, Y. Sato, S. Inoue, *Chem. Lett.* **1990**, *19*, 551–554.
[20] I. M. Arafa, K. Shin, H. M. Goff, *J. Am. Chem. Soc.* **1988**, *110*, 5228–5229.
[21] P. Cocolios, R. Guilard, D. Bayeul, C. Lecomte, *Inorg. Chem.* **1985**, *24*, 2058–2062.
[22] T. Ema, Y. Miyazaki, S. Koyama, Y. Yano, T. Sakai, *Chem. Commun.* **2012**, *48*, 4489–4491.
[23] L. Jin, H. Jing, T. Chang, X. Bu, L. Wang, Z. Liu, *J. Mol. Catal. A* **2007**, *261*, 262–267.
[24] K. Kasuga, N. Moriwaki, M. Handa, *Inorg. Chim. Acta* **1996**, *244*, 137–139.
[25] J. Weidlein, *Z. Anorg. Allg. Chem.* **1970**, *378*, 245–262.
[26] K. Ziegler, *Justus Liebigs Ann. Chem.* **1960**, *629*, 251.
[27] A. Caise, D. Jones, E. L. Kolychev, J. Hicks, J. M. Goicoechea, S. Aldridge, *Chem. Eur. J.* **2018**, *24*, 13624–13635.
[28] E. Theuergarten, J. Schlosser, D. Schluns, M. Freytag, C. G. Daniliuc, P. G. Jones, M. Tamm, *Dalton Trans.* **2012**, *41*, 9101–9110.
[29] A. Berkefeld, W. E. Piers, M. Parvez, *J. Am. Chem. Soc.* **2010**, *132*, 10660–10661.
[30] A. E. Ashley, A. L. Thompson, D. O'Hare, *Angew. Chem. Int. Ed.* **2009**, *48*, 9839–9843; *Angew. Chem.* **2009**, *121*, 10023.
[31] C. M. Mömming, E. Otten, G. Kehr, R. Fröhlich, S. Grimme, D. W. Stephan, G. Erker, *Angew. Chem. Int. Ed.* **2009**, *48*, 6643–6646; *Angew. Chem.* **2009**, *121*, 6770.
[32] D. W. Stephan, G. Erker, *Angew. Chem. Int. Ed.* **2015**, *54*, 6400–6441; *Angew. Chem.* **2015**, *127*, 6498.
[33] F. Bertini, V. Lyaskovskyy, B. J. J. Timmer, F. J. J. de Kanter, M. Lutz, A. W. Ehlers, J. C. Slootweg, K. Lammertsma, *J. Am. Chem. Soc.* **2012**, *134*, 201–204.
[34] U. Gellrich, *Angew. Chem. Int. Ed.* **2018**, *57*, 4779–4782; *Angew. Chem.* **2018**, *130*, 4869.
[35] M. A. Courtemanche, M. A. Legare, L. Maron, F. G. Fontaine, *J. Am. Chem. Soc.* **2013**, *135*, 9326–9329.
[36] R. Declercq, G. Boudahir, D. Bourissou, M. A. Legare, M. A. Courtemanche, K. S. Nahi, N. Bouchard, F. G. Fontaine, L. Maron, *ACS Catal.* **2015**, *5*, 2513–2520.
[37] M. A. Courtemanche, A. P. Pulis, E. Rochette, M. A. Legare, D. W. Stephan, F. G. Fontaine, *Chem. Commun.* **2015**, *51*, 9797–9800.
[38] L. J. Murphy, K. N. Robertson, R. A. Kemp, H. M. Tuononen, J. A. C. Clyburne, *Chem. Commun.* **2015**, *51*, 3942–3956.
[39] S. Shyshkanov, T. N. Nguyen, A. Chidambaram, K. C. Stylianou, P. J. Dyson, *Chem. Commun.* **2019**, *55*, 10964–10967.
[40] G. Ménard, D. W. Stephan, *J. Am. Chem. Soc.* **2010**, *132*, 1796–1797.
[41] G. Ménard, D. W. Stephan, *Angew. Chem. Int. Ed.* **2011**, *50*, 8396–8399; *Angew. Chem.* **2011**, *123*, 8546.
[42] T. Holtrichter-Rößmann, J. Isermann, C. Rosener, B. Cramer, C. G. Daniliuc, J. Kosters, M. Letzel, E. U. Wurthwein, W. Uhl, *Angew. Chem. Int. Ed.* **2013**, *52*, 7135–7138; *Angew. Chem.* **2013**, *125*, 7275.
[43] F. Hengesbach, X. Jin, A. Hepp, B. Wibbeling, E. U. Wurthwein, W. Uhl, *Chem. Eur. J.* **2013**, *19*, 13901–13909.
[44] K. Martinewski, T. Holtrichter-Rossmann, C. Rosener, A. Hepp, E. U. Wurthwein, W. Uhl, *Chem. Eur. J.* **2017**, *23*, 6129–6141.
[45] S. Roters, C. Appelt, H. Westenberg, A. Hepp, J. C. Slootweg, K. Lammertsma, W. Uhl, *Dalton Trans.* **2012**, *41*, 9033–9045.
[46] C. Appelt, H. Westenberg, F. Bertini, A. W. Ehlers, J. C. Slootweg, K. Lammertsma, W. Uhl, *Angew. Chem. Int. Ed.* **2011**, *50*, 3925–3928; *Angew. Chem.* **2011**, *123*, 4011.
[47] M. Layh, W. Uhl, G. Bouhadir, D. Bourissou. *Organoaluminum Compounds and Lewis Pairs* in *The Chemistry of Organoaluminum Compounds* (Eds.: L. Micouin, I. Marek, Z. Rappoport). John Wiley and Sons, Hoboken, NJ, **2017**, pp. 379–424.
[48] N. Aders, L. Keweloh, D. Pleschka, A. Hepp, M. Layh, F. Rogel, W. Uhl, *Organometallics* **2019**, *38*, 2839–2852.
[49] C. Appelt, J. C. Slootweg, K. Lammertsma, W. Uhl, *Angew. Chem. Int. Ed.* **2013**, *52*, 4256–4259; *Angew. Chem.* **2013**, *125*, 4350.
[50] M. Lange, J. C. Tendyck, P. Wegener, A. Hepp, E. U. Wurthwein, W. Uhl, *Chem. Eur. J.* **2018**, *24*, 12856–12868.
[51] F. Bertini, C. Hoffmann, C. Appelt, W. Uhl, A. W. Ehlers, J. C. Slootweg, K. Lammertsma, *Organometallics* **2013**, *32*, 6764–6769.
[52] J. Boudreau, M. A. Courtemanche, F. G. Fontaine, *Chem. Commun.* **2011**, *47*, 11131–11133.

[53] M. Courtemanche, J. Larouche, M. Legare, W. Bi, L. Maron, F. Fontaine, *Organometallics* **2013**, *32*, 6804–6811.
[54] F. G. Fontaine, E. Rochette, *Acc. Chem. Res.* **2018**, *51*, 454–464.
[55] F. G. Fontaine, M. A. Courtemanche, M. A. Legare, E. Rochette, *Coord. Chem. Rev.* **2017**, *334*, 124–135.
[56] F. G. Fontaine, M. A. Courtemanche, M. A. Legare, *Chem. Eur. J.* **2014**, *20*, 2990–2996.
[57] N. C. Smythe, D. A. Dixon, E. B. Garner III, M. M. Rickard, M. Mendez, B. L. Scott, B. Zelenay, A. D. Sutton, *Inorg. Chem. Commun.* **2015**, *61*, 207–209.
[58] T. Habereder, H. Noth, R. T. Paine, *Eur. J. Inorg. Chem.* **2007**, 4298–4305.
[59] J. Chen, L. Falivene, L. Caporaso, L. Cavallo, E. Y. X. Chen, *J. Am. Chem. Soc.* **2016**, *138*, 5321–5333.
[60] H. S. Zijlstra, J. Pahl, J. Penafiel, S. Harder, *Dalton Trans.* **2017**, *46*, 3601–3610.
[61] M. Devillard, R. Declercq, E. Nicolas, A. W. Ehlers, J. Backs, N. SaffonMerceron, G. Bouhadir, J. C. Slootweg, W. Uhl, D. Bourissou, *J. Am. Chem. Soc.* **2016**, *138*, 4917–4926.
[62] J. Takaya, N. Iwasawa, *J. Am. Chem. Soc.* **2017**, *139*, 6074–6077.
[63] N. J. DeYonker, C. E. Webster, *Inorg. Chim. Acta* **2015**, *436*, 220–229.
[64] S. Habershon, *J. Chem. Theory Comput.* **2016**, *12*, 1786–1798.
Farkas, J. B. Foresman, J. V. Ortiz, J. Cioslowski, D. J. Fox, GAUSSIAN 16, Revision B.01; Gaussian Inc., Wallingford, CT. **2016**.
[71] R. G. Parr, W. Yang, *Density Functional Theory of Atoms and Molecules*; Oxford University Press: New York, **1989**.
[72] A. Becke, *J. Chem. Phys.* **1993**, *98*, 5648–5652.
[73] P. Hay, W. Wadt, *J. Chem. Phys.* **1985**, *82*, 299–310.
[74] P. Hay, W. Wadt, *J. Chem. Phys.* **1985**, *82*, 270–283.
[65] R. M. Charles III, T. W. Yokley, N. D. Schley, N. J. DeYonker, T. P. Brewster, *Inorg. Chem.* **2019**, *58*, 12635–12645.
[66] R. G. Letterman, C. B. Duke III, T. T. To, T. J. Burkey, C. E. Webster, *Organometallics* **2014**, *33*, 5928–5931.
[67] G. R. Fulmer, A. J. M. Miller, N. H. Sherden, H. E. Gottlieb, A. Nudelman, B. M. Stoltz, J. E. Bercaw, K. I. Goldberg, *Organometallics* **2010**, *29*, 2176–2179.
[68] OLEX2: O. V. Dolomanov, L. J. Bourhis, R. J. Gildea, J. A. K. Howard, H. Puschmann, *J. Appl. Crystallogr.* **2009**, *42*, 339–341.
[69] SHLEX. G. A. Sheldrick, *Acta Crystallogr., Sect. A* **2008**, *64*, 112–122.
[70] M. J. Frisch, G. W. Trucks, H. B. Schlegel, G. E. Scuseria, M. A. Robb, J. R. Cheeseman, G. Scalmani, V. Barone, B. Mennucci, G. A. Petersson, H. Nakatsuji, M. Caricato, X. Li, H. P. Hratchian, A. F. Izmaylov, J. Bloino, G. Zheng, J. L. Sonnenberg, M. Hada, M. Ehara, K. Toyota, R. Fukuda, J. Hasegawa, M. Ishida, T. Nakajima, Y. Honda, O. Kitao, H. Nakai, T. Vreven, J. A. Montgomery Jr., J. E. Peralta, F. Ogliaro, M. Bearpark, J. J. Heyd, E. Brothers, K. N. Kudin, V. N. Staroverov, R. Kobayashi, J. Normand, K. Raghavachari, A. Rendell, J. C. Burant, S. S. Iyengar, J. Tomasi, M. Cossi, N. Rega, J. M. Millam, M. Klene, J. E. Knox, J. B. Cross, V. Bakken, C. Adamo, J. Jaramillo, R. Gomperts, R. E. Stratmann, O. Yazyev, A. J. Austin, R. Cammi, C. Pomelli, J. W. Ochterski, R. L. Martin, K. Morokuma, V. G. Zakrzewski, G. A. Voth, P. Salvador, J. J. Dannenberg, S. Dapprich, A. D. Daniels, Ö.
[75] P. C. Hariharan, J. A. Pople, *Theor. Chim. Acta* **1973**, *28*, 213–222.
[76] V. Barone, M. Cossi, *J. Phys. Chem. A* **1998**, *102*, 1995–2001.
[77] M. Cossi, N. Rega, G. Scalmani, V. Barone, *J. Comput. Chem.* **2003**, *24*, 669–681.

Received: May 4, 2020

Carbon Dioxide Activation

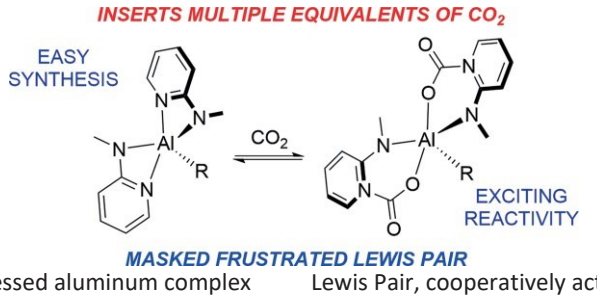

An easily accessed aluminum complex is found to sequester 2–3 equivalents of CO_2 per aluminum center under mild conditions. The aluminum complex functions as a masked Frustrated Lewis Pair, cooperatively activating the CO_2 substrate. Additional direct insertion of CO_2 into an ethyl ligand is observed at room temperature without the addition of additives.

doi.org/10.1002/ejic.202000437